Title

The Indigenous South American Tsimane Exhibit Relatively Modest Decrease in Brain Volume With Age Despite High Systemic Inflammation

Journal

The Journals of Gerontology Series A, 76(12)

ISSN

1079-5006

Authors

Irimia, Andrei

Chaudhari, Nikhil N

Robles, David J

et al.

Publication Date

2021-11-15

DOI

10.1093/gerona/glab138

Peer reviewed

THE GERONTOLOGICAL SOCIETY OF AMERICA®

Journals of Gerontology: Biological Sciences
cite as: *J Gerontol A Biol Sci Med Sci*, 2021, Vol. 76, No. 12, 2147–2155
doi:10.1093/gerona/glab138
Advance Access publication May 26, 2021

OXFORD

Original Article

The Indigenous South American Tsimane Exhibit Relatively Modest Decrease in Brain Volume With Age Despite High Systemic Inflammation

Andrei Irimia, PhD,[1,2,*] Nikhil N. Chaudhari, MS,[1] David J. Robles, MA,[1] Kenneth A. Rostowsky, BS,[1] Alexander S. Maher, MS,[1] Nahian F. Chowdhury, BS,[1] Maria Calvillo, MA,[1] Van Ngo, BS,[1] Margaret Gatz, PhD,[3] Wendy J. Mack, PhD,[4] E. Meng Law, MD,[5,6,7] M. Linda Sutherland, MD,[8] James D. Sutherland, MD,[8] Christopher J. Rowan, MD,[9,10] L. Samuel Wann, MD,[11] Adel H. Allam, MD,[12] Randall C. Thompson, MD,[13] David E. Michalik, DO,[14,15] Daniel K. Cummings, PhD,[16,17] Edmond Seabright, PhD,[16] Sarah Alami, MA,[18] Angela R. Garcia, PhD,[19] Paul L. Hooper, PhD,[16] Jonathan Stieglitz, PhD,[20] Benjamin C. Trumble, PhD,[19] Michael D. Gurven, PhD,[18] Gregory S. Thomas, MD,[8,21] Caleb E. Finch, PhD,[1,22] and Hillard Kaplan, PhD[17]

[1]Ethel Percy Andrus Gerontology Center, Leonard Davis School of Gerontology, University of Southern California, Los Angeles, USA. [2]Corwin D. Denney Research Center, Department of Biomedical Engineering, University of Southern California, Los Angeles, USA. [3]Center for Economic and Social Research, Dana and David Dornsife College of Letters, Arts and Sciences, University of Southern California, Los Angeles, USA. [4]Department of Preventive Medicine, Keck School of Medicine, University of Southern California, Los Angeles, USA. [5]iBRAIN Research Laboratory, Departments of Neuroscience, Computer Systems and Electrical Engineering, Monash University, Melbourne, Victoria, Australia. [6]Department of Radiology, The Alfred Health Hospital, Melbourne, Victoria, Australia. [7]Department of Neurology, Keck School of Medicine of USC, University of Southern California, Los Angeles, USA. [8]MemorialCare Heart & Vascular Institute, Fountain Valley, California, USA. [9]Renown Institute for Heart and Vascular Health, Reno, Nevada, USA. [10]School of Medicine, University of Nevada, Reno, USA. [11]Ascension Healthcare, Milwaukee, Wisconsin, USA. [12]Department of Cardiology, School of Medicine, Al-Azhar University, Al Mikhaym Al Daem, Cairo, Egypt. [13]Saint Luke's Mid America Heart Institute, University of Missouri, Kansas City, USA. [14]Department of Pediatrics, School of Medicine, University of California at Irvine, Orange, USA. [15]MemorialCare Miller Children's & Women's Hospital, Long Beach Medical Center, California, USA. [16]Department of Anthropology, University of New Mexico, Albuquerque, USA. [17]Economic Science Institute, Argyros School of Business and Economics, Chapman University, Orange, California, USA. [18]Department of Anthropology, University of California, Santa Barbara, USA. [19]Center for Evolution & Medicine, School of Human Evolution and Social Change, Arizona State University, Tempe, USA. [20]Institute for Advanced Study in Toulouse, Toulouse 1 Capitol University, France. [21]Division of Cardiology, University of California, Irvine, Orange, USA. [22]Departments of Biological Sciences, Anthropology and Psychology, Dana and David Dornsife College of Letters, Arts and Sciences, University of Southern California, Los Angeles, USA.

*Address correspondence to: Andrei Irimia, PhD, Ethel Percy Andrus Gerontology Center, Leonard Davis School of Gerontology, University of Southern California, 3715 McClintock Avenue, Suite 228, Los Angeles, CA 90089, USA. E-mail: irimia@usc.edu

Received: January 12, 2021; Editorial Decision Date: April 22, 2021

Decision Editor: David Le Couteur, MBBS, FRACP, PhD

Abstract

Brain atrophy is correlated with risk of cognitive impairment, functional decline, and dementia. Despite a high infectious disease burden, Tsimane forager-horticulturists of Bolivia have the lowest prevalence of coronary atherosclerosis of any studied population and present few cardiovascular disease (CVD) risk factors despite a high burden of infections and therefore inflammation. This study (a) examines the

statistical association between brain volume (*BV*) and age for Tsimane and (b) compares this association to that of 3 industrialized populations in the United States and Europe. This cohort-based panel study enrolled 746 participants aged 40–94 (396 males), from whom computed tomography (CT) head scans were acquired. *BV* and intracranial volume (*ICV*) were calculated from automatic head CT segmentations. The linear regression coefficient estimate $\hat{\beta}_T$ of the Tsimane (*T*), describing the relationship between age (predictor) and *BV* (response, as a percentage of *ICV*), was calculated for the pooled sample (including both sexes) and for each sex. $\hat{\beta}_T$ was compared to the corresponding regression coefficient estimate $\hat{\beta}_R$ of samples from the industrialized reference (*R*) countries. For all comparisons, the null hypothesis $\beta_T = \beta_R$ was rejected both for the combined samples of males and females, as well as separately for each sex. Our results indicate that the Tsimane exhibit a significantly slower decrease in *BV* with age than populations in the United States and Europe. Such reduced rates of *BV* decrease, together with a subsistence lifestyle and low CVD risk, may protect brain health despite considerable chronic inflammation related to infectious burden.

Keywords: Brain aging, Cardiovascular disease, Neurodegeneration

Ageing-related brain atrophy is strongly associated with elevated risk of cognitive impairment, functional decline, and dementia, and is moderated by factors like diet, smoking, and physical activity. Brain atrophy trajectories are positively associated with cardiovascular disease (CVD) risk factors (1) such as high cholesterol, diabetes, and hypertension, which are widespread in modern, industrialized populations (2). Thus, populations with a lower prevalence of CVD risk factors are hypothesized to exhibit *slower* brain volume (*BV*) loss and lower risk for associated cognitive decline. On the other hand, populations with high infectious and inflammatory burdens are hypothesized to exhibit *faster BV* loss (3,4) because systemic inflammation predicts greater brain atrophy (5–7).

Indigenous Tsimane forager-horticulturists of lowland Bolivia have a lifestyle similar to that of subsistence populations prior to mechanized agriculture, urbanization, and industrialization. The ~16 000 members of this population live by farming, hunting, gathering, and fishing in the Amazon basin, and have a documented high burden of infections and inflammation (8), including increased systemic inflammation (9). This is reflected by their biomarkers of chronic immune activation, including higher leukocytes counts, faster erythrocyte sedimentation rates, and higher levels of C-reactive protein (9), interleukin-6, and immunoglobulin-E (10) than in Americans of all ages (9,11,12). The Tsimane feature endemic polyparasitism involving helminths (13) and frequent gastrointestinal illness; most morbidity and mortality in this population being due to infections (9,14). The higher inflammatory burden among the Tsimane suggests the hypothesis that they exhibit *steeper* negative associations between *BV* and age compared to populations with relatively lower systemic inflammation. Despite their inflammatory load, however, Tsimane have the lowest prevalence of coronary atherosclerosis of any studied population (8) and present few CVD risk factors like hypertension (15), obesity, type 2 diabetes, and hyperlipidemia (16,17). Additionally, Tsimane have CVD protective factors like high levels of physical activity starting early in life (18), and a diet that is rich in fiber, omega-3 fatty acids, and polyunsaturated fatty acids (19), but low in saturated fats and preservatives (20). Thus, to the extent that CVD and cognitive decline risk factors are shared (21), one might hypothesize a shallower negative association between *BV* and age for Tsimane compared to industrialized populations. These divergent hypotheses were tested in this cohort-based panel study.

Method

Study Design and Participants

The Tsimane Health and Life History Project team has been studying the Tsimane since 2002, covering 85 villages and sampling persons aged 40 or older in a cohort-based panel design. The team visits Tsimane villages regularly and undertakes clinical examinations to study within- and cross-population variations in aging, including studies of infections and inflammation, coronary atherosclerosis, diet, and physical activity, as described above. The cross-sectional sample of this study includes individuals who self-identified as Tsimane and who were aged between 40 and 94. The Tsimane exhibit a pyramidal population structure, with relatively fewer persons aged older than 60. For this reason, all individuals older than 60 were screened for enrollment. Potential participants aged 40–59 were identified for screening at the community—rather than individual—level. This approach was adopted for reasons of cultural appropriateness, so that no potential volunteer would feel either targeted or excluded. All Tsimane older than 60 participated except for 85 individuals; 9 declined to participate, 17 were not in their home communities at the time of the study, 9 were busy with subsistence activities, 1 person was hospitalized, and 49 individuals wanted to participate in the future but had prior obligations at the time of scanning. There were no significant differences in age or sex for participants and nonparticipants older than 60 (age: $t_{103} = 1.98$, Cohen's $d = 0.27$, $p = .95$; sex: $t_{114} = -0.81$, Cohen's $d = -0.10$, $p = .58$). A total of 746 participants (396 males) participated in the study. Included were 143 participants younger than 50, 239 aged between 50 and 59, 226 aged between 60 and 69, 105 aged between 70 and 79, 29 aged between 80 and 89, and 4 aged 90 years or older. Participants were compensated for their time.

Computed Tomography Acquisition

Participants were bussed to the city of Trinidad, Bolivia, whose computed tomography (CT) imaging facility is closest to the Tsimane villages. Although magnetic resonance imaging (MRI) would have been preferable to CT, providing participants with transportation to an MRI scanner facility was not logistically feasible. A licensed radiological technician acquired head CT scans using a 16-detector row scanner (GE BrightSpeed, Milwaukee, WI). At least 3 team clinicians supervised and reviewed the scans. Images were acquired clockwise, in helical mode, with a standard convolution kernel, and with 2 reconstructions: one with a voxel size of 1.25 mm × 1.25 mm × 1.25 mm, and another with a voxel size of 0.625 mm × 0.625 mm × 0.625 mm. Additional parameters included a kilovoltage peak of 120 kV, a data collection diameter of 250 mm, a mean exposure time of 1 417 ms, an x-ray tube current of 140 mA, and a focal spot of 0.7 mm.

CT Segmentation

CT volumes were segmented as described extensively elsewhere (22). Briefly, a probabilistic classification method (23) was used to

perform tissue classification; voxel intensity values were used to assign their probabilities of belonging to one of several tissue classes by estimating the intensity distributions parameters of each class. The segmentation approach assigns each CT voxel in the cranium to either *BV*, or cerebrospinal fluid volume (*CSFV*), such that intracranial volume (*ICV*) = *BV* + *CSFV*. The distribution of image intensities was modeled by a mixture of clusters, each consisting of Gaussian random variables (24). By estimating the parameters of the intensity distributions for each class, voxel intensity information can be used to assign each voxel a probability of belonging to each tissue class. First, an objective function derived from a mixture of Gaussian random variable models is derived, and the value of this function is minimized using a parameter optimization process. A priori tissue probability maps specified by an atlas are leveraged to assist this classification. This probabilistic atlas is used to specify the prior probability for each voxel to belong to any tissue class in the Gaussian mixture model. The objective function weighs the probability maps of the atlas using Bayesian inference and then deforms the maps so that they match the volumes to be segmented. At this stage, the atlas template is warped to each subject's *BV* (25), the latter is segmented and the spatial classifications are smoothed (26). Model parameters are optimized using an expectation maximization algorithm (24), where the Gaussian mixture and deformations are reassessed iteratively and deformations are optimized using a Gauss–Newton scheme (27). When integrated with a priori information provided by the template, Bayesian inference facilitates the calculation of posterior probabilities based on each subject's voxel intensities.

CT-to-MRI Validation

We validated our CT segmentation approach using a sample of 24 U.S. adults aged 54–75 who had both MRI and CT scans of the head. In this validation study, CT scan parameters and spatial resolution were like those of the CTs acquired from the Tsimane. T_1-weighted MRI volumes were acquired at 3 T in a Prisma MAGNETOM Trio TIM scanner (Siemens Corp., Erlangen, Germany) using a magnetization-prepared rapid acquisition gradient echo sequence with the following parameters: repetition time (T_R) = 1 950 ms; echo time (T_E) = 3 ms; inversion time (T_I) = 900 ms; flip angle (FA) = 9 degrees; percentage sampling = 100; pixel bandwidth (BW) = 240 Hz/pixel; matrix size = 256 × 256; voxel size = 1 mm × 1 mm × 1 mm. In the CT-to-MRI comparison, CT segmentations were validated against MRI segmentations which had been implemented using Freesurfer 7.0 software, as detailed elsewhere (22). Three quantitative measures were calculated: (a) the Sørensen–Dice coefficient (conveying the overlap between CT and MRI tissue labeling maps), (b) the Hausdorff distance (a measure of how far the CT- and MR-based boundaries are between tissues), and (c) the intraclass correlation coefficient (a metric of measurement reproducibility which is useful when distinct techniques are used to measure the same empirical quantity). The Sørensen–Dice coefficient was found to have a Gaussian distribution with mean μ = 89.3% and standard deviation σ = 0.85% for the brain; for ventricular CSF, μ = 92.2% and σ = 0.175%. The average Hausdorff distance and its ±2σ interval were 2.1 ± 0.9 mm for the brain, and 2.5 ± 1.3 mm for ventricular CSF. The intraclass correlation coefficient was 0.78 for the brain and 0.74 for CSF. Together, these metrics were found to indicate segmentation quality which was adequate for the purpose of *BV* calculations. Across the entire validation sample, the mean percentage difference between CT- and MRI-based volumetrics and its ±2σ interval were found to be ~0% ± 3.2% for *BV* and ~0% ± 2.6% for *CSFV*. Thus, on average in this small sample, our CT- and MRI-derived measures differ by a negligible amount, confirming that the CT-based volumetrics can be compared to the MRI-based measures with little average intermodality error.

Tsimane Comparison to Other Cohorts

We compared the Tsimane regression coefficients β_T to those calculated from 2 MRI studies of aging. The first study, by Schippling et al. (28), involved 564 participants scanned in either Hamburg, Germany (*N* = 248) or St. Louis, United States (*N* = 316). This study was included partly because it utilized a segmentation technique for MRI scans similar to ours used for CT scans, which adds to the comparability of β_T and β_R. The second study, by Vinke et al. (29), investigated 5 286 participants in the Rotterdam Study, a population-based study of age-related diseases. Both Schippling et al. and Vinke et al. analyzed MRIs with voxel sizes equal or less than 1 mm^3, thus satisfying the typical spatial resolution requirements of today's MRI studies.

For statistical comparison of our *BV* trajectories to those of Schippling et al. and Vinke et al., we compared their slopes using linear models. For Schippling et al., who had provided regression coefficients for 5-year age intervals, β_R was computed as a weighted average over the age interval from 40 to 70 years. Weights equaled the values of the empirical probability density function associated with the ages of Tsimane participants, thereby allowing us to eliminate the potential confounding effect of differences in age distributions across cohorts. For Vinke et al., β_R was calculated based on the volumetric trajectories and data reported in Figure 1A and in Table 3 of this publication. The volumetric trajectories of Vinke et al. are approximately linear within the age intervals [45, 70] and [70, 95] years. Within each of these intervals, β_R is, therefore, well approximated by $\Delta V/\Delta t = [V(a_2) - V(a_1)]/(a_2 - a_1)$, that is, by the difference in volume *V* divided by the difference in age *a* across the interval from a_1 to a_2. The value of β_R within the full interval [45, 95] years was calculated as the average value of $\Delta V/\Delta t$ over the intervals [45, 70] and [70, 95] years. Although neither reference study reports their model parameters, both report nonlinear relationships with age. For this reason, we explore nonlinear (quadratic) models for illustration (Figure 1B); the reader is referred to the study of Irimia (30) for further quantitation, comparison, and meta-analysis of both linear and nonlinear models for *BV*, WM volume (*WMV*), GM volume (*GMV*), and *CSFV*.

To gain insight into potential neuroanatomic differences between the Tsimane and the reference populations as a function of age, 3 representative Tsimane female subjects (ages: 40, 60, and 80 years, respectively) were selected. Three CT scan slices (axial, sagittal, and coronal) from each subject were collated for illustration of typical age effects upon brain features within the sample (Figure 2). To highlight how such features can reflect discrepancies between Tsimane and the reference populations, we also selected 2 Tsimane subjects aged 80, one whose *BV* was closest to the regression line for the Tsimane (see continuous red trace in Figure 1A), and another whose *BV* was closest to the regression line for the reference population (see continuous black trace in Figure 1A). Although both subjects are Tsimane, the latter subject's brain CT features are representative of the neuroanatomic profile of an 80-year-old subject in the reference population. The comparison between the 2 subjects is illustrated in Figure 3.

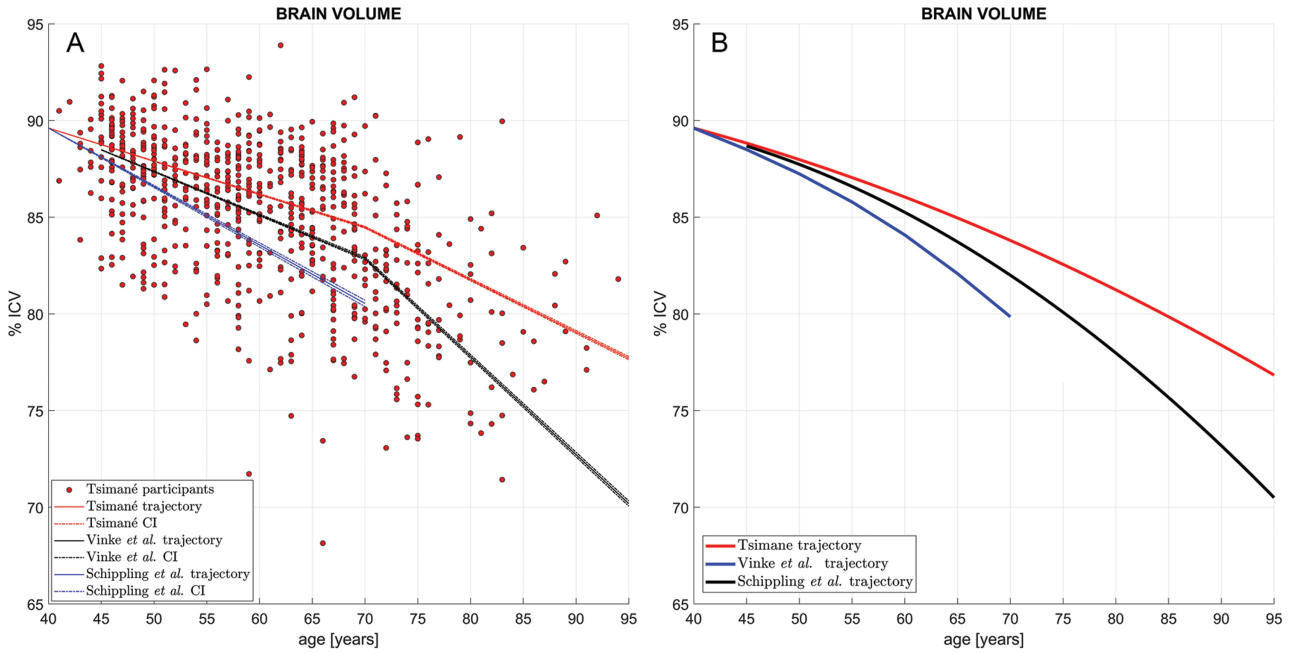

Figure 1. (**A**) Cross-sectional brain volume (*BV*) as a percentage of intracranial volume (*ICV*) and its age-dependent linear trajectories in the Tsimane (red), in the reference sample of Schippling et al. (blue) and in that of Vinke et al. (black). Dots represent Tsimane participants' *BV*s. Dash-dotted lines mark the range of trajectories within the confidence interval (CI) of the bootstrapping-estimated regression coefficient estimate $\hat{\beta}$ (*not* within the CI of the *BV* measurements themselves). The Tsimane and reference samples are assumed to have the same mean *BV* at ages 40 y, to facilitate comparison of their slopes and to obviate the divergence of trajectories as a function of age. Note the small CIs of $\hat{\beta}$ across the magnetic resonance imaging reference samples and the substantial divergence of the Tsimane CI (red) from it, particularly after age ~70 y. The null hypothesis $\beta_T = \beta_R$ fails to be accepted both on the interval 40–70 y (Tsimane vs Schippling et al. (28): $t_{3388} = -75.47$, $p \simeq 1.0 \times 10^{-250}$, power ≃ 99%; Tsimane vs Vinke et al.: $t_{1477} = -60.89$, $p \simeq 1.0 \times 10^{-250}$, power ≃ 99%) and on the interval 70–95 y (Tsimane vs Vinke et al.: $t_{1516} = -424.05$, $p \simeq 1.0 \times 10^{-250}$, power ≃ 99%). (**B**) Similar to (A), comparing quadratic models of *BV* trajectories as a function of age in the Tsimane (red) against quadratic models of the trajectories in Schippling et al. (blue) and in Vinke et al. (29) (black). CIs and data points for individual Tsimane *BV* values are omitted to facilitate comparison. The curvilinear fit to the Tsimane data confirms and reproduces a slower rate of *BV* decrease in the Tsimane after age 70, in contrast to the reference samples, where faster rates of cross-sectional *BV* decline are observed.

Statistical Analysis

Ages were centered on their means prior to statistical analysis. We implemented univariate linear regressions to test the null hypothesis that the Tsimane linear regression coefficient β_T describing the association between age (predictor variable) and *ICV*-adjusted *BV* is equal to zero. Two-tailed Welch's *t* tests were used. The significance of sex as a predictor was explored, the age association was tested both across sexes and within each sex group, and the significance of the sex-by-age interaction was investigated. Statistical analyses of Tsimane data were implemented using IBM SPSS software, version 27.

The linear regression coefficients β_T of the Tsimane (describing associations between age and volumetrics) were compared against regression coefficients β_R reported elsewhere (28,29) for samples from 3 industrialized countries (Germany, United States, and the Netherlands, see Tsimane Comparison to Other Cohorts). The null hypothesis $\beta_T = \beta_R$ was tested both within the full age interval [40, 95] years and within each of the intervals [40, 70] and [70, 95] years. For *BV*, the null hypothesis $\beta_T = \beta_R$ was tested at a significance threshold α of 0.05 using Welch's two-tailed *t* test for independent samples with unequal variances. Regression coefficients were assumed to be normally distributed.

The variance estimates of the regression coefficients β_T and β_R were obtained via bootstrapping using 10 000 simulations. In each simulation, a random subsample *S* of size 300 was drawn from the set of Tsimane participants' ages, thus allowing $\sigma(\beta_R)$ to be estimated without the potentially confounding effect of age distribution differences between the Tsimane and the simulated samples. Then, for a simulated set of Western subjects with ages specified by *S*, *ICV*-normalized *BV* values were simulated, assuming that these volumes were normally distributed with parameters μ and σ equal to those reported by each of the 2 reference studies (ie, Schippling et al. (28) and Vinke et al. (29)). In other words, for each reference study, each sample of simulated volumes had the same distribution as those in the reference sample, and the ages of the subjects whose volumes were simulated were those in the subset *S* of 300 subjects selected at random from the Tsimane sample. The regression coefficient estimate $\hat{\beta}_R$ was then calculated for each such realization. After 10 000 realizations, we then computed the estimates $\hat{\mu}(\beta_R)$ and $\hat{\sigma}(\beta_R)$, that is, the estimated parameters of the normally distributed, *ICV*-normalized *BV* values reported by the reference study in question.

Once $\mu(\beta_R) \simeq \beta_R$ and $\sigma(\beta_R)$ had been estimated, the null hypothesis $\beta_R = \beta_T$ was tested using Welch's *t* test. For all simulations, the error of the Tsimane participants' recorded ages was assumed to be normally distributed with zero mean and a worst-case-scenario value of σ equal to 1.5 years. This assumption was made because Tsimane birth records are occasionally inaccurate by up to 3 years (14). Similarly, to reflect uncertainties in the accuracy of CT-derived brain segmentations, the measurement error associated with *BV* was assumed to be normally distributed ($\hat{\sigma} = 0\%$, $\hat{\sigma} = 0.8\%$), corresponding to a measurement error interval $[-2\hat{\sigma}, 2\hat{\sigma}]$ equal to [–3.2, 3.2] %, as observed empirically during validation (see also *CT-to-MRI Validation*). The approach described above was used to estimate $\mu(\beta_I)$ and $\sigma(\beta_I)$ for each reference cohort. Bootstrapping

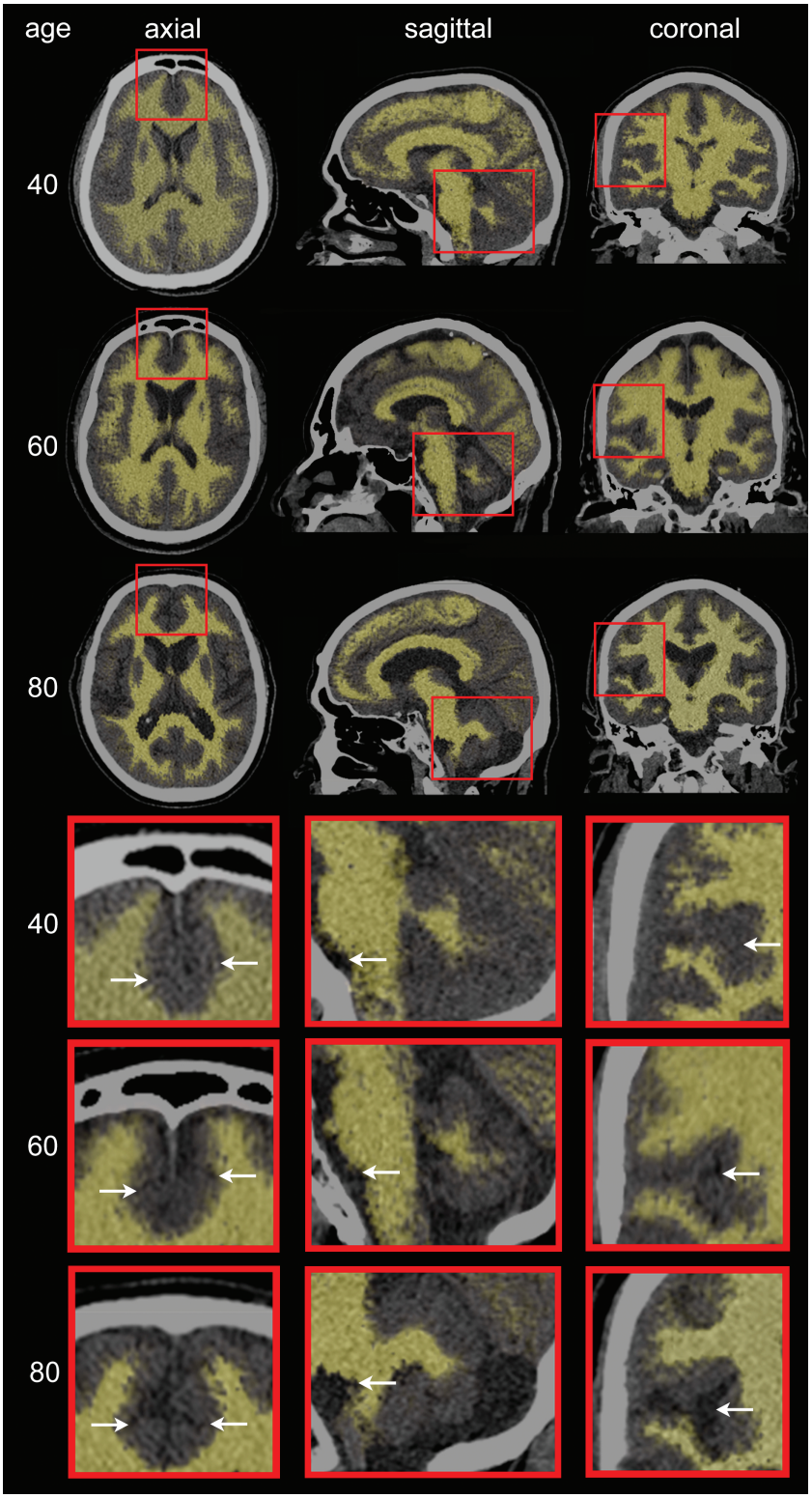

Figure 2. Axial, sagittal, and coronal computed tomography (CT) slices for 3 representative Tsimane subjects (3 females of ages 40, 60, and 80 y, respectively). Typical aging effects upon the gray matter (GM) and white matter (WM) are highlighted, with WM depicted by semi-transparent beige overlays superimposed onto the CT scan images. GM aging features include overall shrinking of the gyri and widening of the sulci, particularly in the medial frontal lobes (axial inset arrows: cingulate sulci), lateral and medial temporal lobes (eg, Sylvian fissures and temporal opercula), parietal lobes (eg, parietal opercula), insulae (coronal inset arrows: circular sulci), and hippocampal formations (eg, choroid fissures and ambient cisterns). WM aging is highlighted by enlargement of cerebrospinal fluid structures (lateral and third ventricles) and by brain stem atrophy (sagittal inset arrows: boundary between the pons and medulla oblongata). Cerebellar atrophy (sagittal inset) reflects both GM and WM loss.

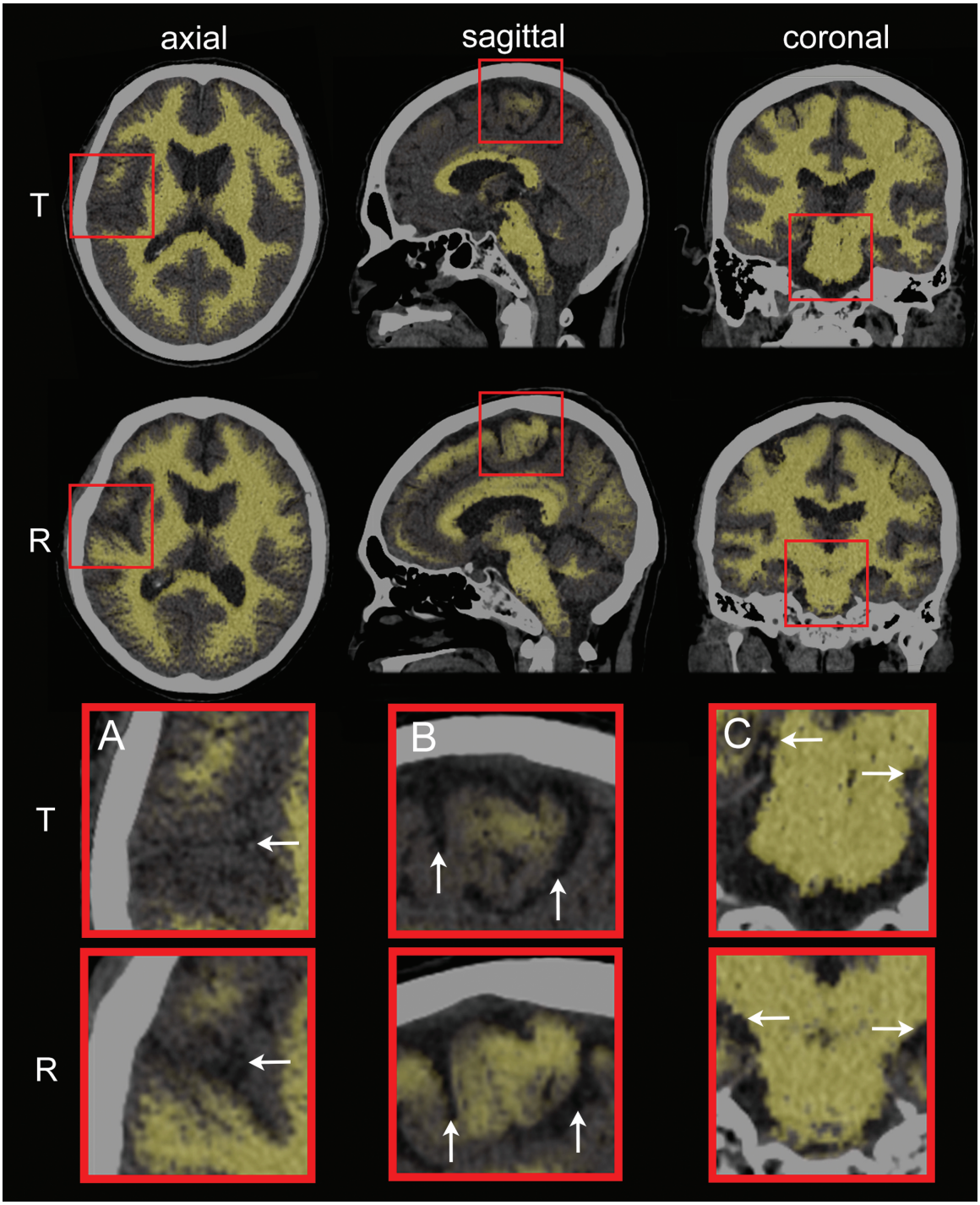

Figure 3. Neuroanatomic differences between a subject representative of the Tsimane trajectory at age 80 y (first row, cf. continuous red trace in Figure 1A) and a subject representative of the reference trajectory at the same age (second row, cf. continuous black trace in Figure 1A). Axial, sagittal, and coronal CT slices are shown for each subject. Key neuroanatomic distinctions between the 2 subjects are highlighted by arrows within each inset and include the extent of atrophy along (A) the circular sulcus of the insula, (**B**) the precentral and central sulci, and (**C**) the hippocampal formation.

simulations and statistical tests comparing the Tsimane to reference cohorts were implemented in MATLAB 2020a. Post-hoc statistical power was calculated using G*Power 3.1.9.4 software. No hierarchical or complex design implementation was applicable to this analysis.

To evaluate the potential effect of mortality selection on the observed relationship between age and *BV* in the Tsimane, a Cox proportional hazards model was fit to the Tsimane brain CT sample data, including terms accounting for sex, age, and *BV* as a percentage of *ICV*. To estimate the effect of differential mortality, we simulated hypothetical trajectories of brain aging with and without mortality selection. This begins with the cohort of Tsimane younger than 60 at scan time and simulates aging and mortality in each subsequent year of life. During each year included in the simulation,

each participant's *BV* atrophies by some specified amount. The expected mortality is then estimated directly from the Cox model and depends on each simulated *BV* and age in each year. Mortality selection occurs as individuals with smaller brains are more likely to be removed from the sample, thereby increasing the average *BV* of remaining participants.

Results

All Tsimane adults aged older than 60 years were invited to enroll, whereas those aged 40–59 were sampled from a subset of representative communities. The study was approved by the University of New Mexico Health Sciences Institutional Review Board (HRRC 07-157; 15-133). After explaining the procedure and risks in the Tsimane language, informed consent was obtained from the Tsimane government, village leadership, and participants. Because MRI was logistically unfeasible, low-radiation dose CT head scans were acquired from 746 participants aged 40–94 (396 males) who had accepted our invitation for transportation to the nearest CT imaging facility. *BV* and *ICV* were calculated from automatic head CT segmentations (22). Volumetrics were normalized by *ICV* (ie, *BV* as percent of *ICV* was calculated) to alleviate the confounding effect of head size.

The linear regression coefficient estimate $\hat{\beta}_T$ of the Tsimane (*T*), describing the relationship between age (predictor) and *BV* (response, as a percentage of *ICV*), was calculated for the pooled sample (including both sexes) and for each sex. $\hat{\beta}_T$ was compared to the corresponding regression coefficient estimate $\hat{\beta}_R$ of samples from 3 industrialized reference (*R*) countries. Specifically, $\hat{\beta}_R$ was extracted from 2 reference MRI studies (28,29) that were the most methodologically comparable to our CT study, based on criteria related to image processing and quality. Schippling et al. (28) had a combined sample (*N* = 564) of healthy volunteers aged 35–75 from Hamburg, Germany (*N* = 248) and St. Louis, United States (*N* = 316). Vinke et al. (29) studied 5 286 neurologically healthy participants from Rotterdam, the Netherlands. The null hypothesis $\beta_T = \beta_R$ was tested at a significance threshold α of 0.05 across each of 2 distinct age intervals (40–70 and 70–95 years), and across the combined age interval 40–95 years. Across a variety of functional and cognitive aging indicators, change accelerates around 70 years (31), which was selected to define the boundary between the former 2 intervals.

Values of $\hat{\beta}_T$ are −0.228%/y for males and −0.200%/y for females (Table 1). The model including both sexes shows a small significant main effect of male sex reducing *BV*; however, the age-by-sex interaction is not significant, indicating that slopes do not differ significantly by sex. Figure 1A shows *ICV*-normalized *BV* and its age-dependent trajectories for Tsimane and for reference samples. On the interval 40–70 years, $\hat{\beta}_T = -0.171$%/y is significantly shallower than $\hat{\beta}_R$, which equals −0.307%/y for Schippling et al. and −0.225%/y for Vinke et al. (Table 2). Strikingly, on the interval 70–95 years, the Rotterdam estimate $\hat{\beta}_R = -0.507$%/y is almost twice the value of $\hat{\beta}_T = -0.271$%/y. The null hypothesis $\beta_T = \beta_R$ was rejected for the entire age interval 40–95 years both for the combined samples of males and females in the 2 reference MRI studies, as well as separately for each sex (Table 3).

Figure 2 displays axial, sagittal, and coronal CT slices from 3 representative Tsimane female subjects of ages 40, 60, and 80, respectively. Visual comparison of these CT slices reveals progressive aging of the GM and WM (arrows). Neuroanatomical features of GM aging include GM volume loss reflected by gyral shrinking and sulcal widening in regions like the medial frontal lobes (cf. inferior frontal sulci), lateral and medial temporal lobes (cf. superior temporal sulci, temporal opercula), parietal lobes (cf. parietal opercula),

Table 1. Regressions of Age and Sex (predictor variables) Against *ICV*-Normalized *BV* (response variable) in the Tsimane

Group	Variable	$\hat{\beta}_T$	SEM	*t*	CI	Partial η^2	Power
M	Intercept	84.801	0.170	499.798	[84.467, 85.134]	0.998	1.000
	Age	−0.228	0.016	−13.893	[−0.260, −0.196]	0.327	1.000
F	Intercept	85.698	0.170	503.324	[85.363, 86.032]	0.999	1.000
	Age	−0.200	0.016	−12.340	[−0.232, −0.168]	0.304	1.000
M and F	Intercept	85.698	0.176	486.484	[85.352, 86.043]	0.997	1.000
	Age	−0.200	0.017	−11.927	[−0.233, −0.167]	0.160	1.000
	Male sex	−0.897	0.241	−3.716	[−1.371, −0.423]	0.018	0.960
	Age × Male sex	−0.028	0.023	−1.191	[−0.073, 0.018]	0.002	0.221

Notes: *BV* = brain volume; *ICV* = intracranial volume. Intercepts, linear regression coefficient estimates ($\hat{\beta}_T$), standard errors of the mean (SEMs), Student's *t* statistics, 95% confidence intervals (CIs), effect sizes (partial η^2), and observed power are reported. *BV* and age are significantly associated both when each sex (M, F) is considered separately, and when the sexes are considered together (M and F). Ages were centered on their mean prior to statistical analysis. For all statistical tests, *p* values are $<1.0 \times 10^{-3}$. The age-by-sex interaction was not found to be significant ($p = .234$) but the test is underpowered (power = 0.221).

Table 2. The Relationship Between Age in Years (predictor) and *ICV*-Normalized *BV* (percentage of *ICV*, response) on the Age Intervals [40, 70], [70, 95], and [40, 95] y, as Described by Linear Regression Coefficient Estimates $\hat{\beta}$ and Their Confidence Intervals (CIs)

Cohort	*N*	Ages	$\hat{\beta}$	CI ($\hat{\beta}$)	Ages	$\hat{\beta}$	CI ($\hat{\beta}$)	Ages	$\hat{\beta}$	CI ($\hat{\beta}$)
Tsimane	746	[40, 70]	−0.1710	[−0.1731, −0.1689]	[70, 95]	−0.2706	[−0.2779, −0.2633]	[40, 95]	−0.2163	[−0.2192, −0.2135]
Schippling et al.	564	[40, 70]	−0.3069	[−0.3124, −0.3014]	[70, 95]	—	—	[40, 95]	—	—
Vinke et al.	5 286	[45, 70]	−0.2246	[−0.2281, −0.2211]	[70, 95]	−0.5071	[−0.5106, −0.5036]	[45, 95]	−0.3649	[−0.3683, −0.3635]

Notes: *BV* = brain volume; *ICV* = intracranial volume. Aside from values for the Tsimane on the age intervals [40, 70], [70, 95], and [40, 95] y, results are also provided for the reference studies of Schippling et al. (28) (on the age interval [40, 70] y) and Vinke et al. (29) (on age intervals [45, 70], [70, 95], and [45, 95] y). Age intervals are in years (y); values of β and their CIs are in %/y. On the age interval [70, 95] y, the latter 2 quantities are not provided for the sample of Schippling et al. because this study did not include subjects older than 75 y.

Table 3. Results of Testing the Statistical Null Hypothesis $\beta_T = \beta_R$ Using Welch's *t* Test for Samples With Unequal Variances

Study	Schippling et al.		Vinke et al.					
Ages	[40, 70] y		[45, 70] y		[70, 95] y		[45, 95] y	
Sex	*t*	*df*	*t*	*df*	*t*	*df*	*t*	*df*
M	−56.99	3961						
F	−81.90	4489						
M and F	−75.47	3388	−60.89	1477	−424.05	1516	−159.05	1469

Notes: The number of degrees of freedom (*df*) was approximated using the Welch–Satterthwaite equation. Results are reported separately for males (M), females (F) and for combined samples including both males and females (M and F). The null hypothesis was tested for the Tsimane against the samples of both Schippling et al. (28) as well as Vinke et al. (29). In the latter case, the null hypothesis could only be tested for the combined samples of males and females (M and F) because Vinke et al. did not state the numbers of males and females in their sample. Furthermore, because the trajectories of Vinke et al. differ substantially across the age intervals [45, 70] and [70, 95] y, the null hypothesis was tested separately within each of these intervals. In all cases, the threshold for statistical significance is $\alpha = 0.05$. All tests have p values $<1.0 \times 10^{-200}$ and power >99%.

Table 4. Cox Proportional Hazards Model for the Tsimane, Including Terms for Male Sex, Age, and *BV* as a Percentage of *ICV*

Parameter	$\hat{\beta}$	HR	*p*
Male sex	−0.0406	1.501	.237
Age (y)	−0.0995	1.105	<.001
BV (%)	−0.0577	0.944	.196

Note: The estimated coefficients $\hat{\beta}$ of the models are reported in addition to hazards ratios (HR) and to *p* values, for a total of 676 Tsimane (37 deaths).

insulae (cf. circular sulci), and hippocampal formations. WM aging features include enlargement of the lateral and third ventricles, as well as brain stem atrophy (eg, at the boundary between the pons and the medulla oblongata, anterosuperior to the olivary nuclei). Cerebellar atrophy reflects both GM and WM loss in this structure.

Figure 3 highlights typical neuroanatomic differences between Tsimane and the reference populations of Vinke et al. (29). This figure displays CT slices from 2 Tsimane subjects of age 80: one subject's *BV* is closest to the Tsimane regression line (see continuous red trace in Figure 1A), whereas the *BV* of the other is closest to the reference regression line (see continuous black trace in Figure 1A). The *BV* of the second subject (who is representative of the reference population) is ~6.5% larger than that of the first subject (who is representative of Tsimane). The comparison highlights the likely typical extent and features of neuroanatomy differences in old age between the Tsimane and the reference population.

The results of the Cox proportional hazards model are summarized in Table 4, which implies that, when *BV* increases by 1%, the mortality hazard decreases by about 5% (hazard ratio = 0.944). Although the effect is not statistically significant ($p = .196$), it is large enough to have potential biological significance, thus justifying the simulation already described to estimate differential mortality effects. The results of this simulation suggest that, when accounting for mortality effects, the observed regression coefficient $\hat{\beta}_T = -0.2163\%/y$ for individuals with ages in the interval [40, 95] years (Table 2) corresponds to a mortality-adjusted coefficient of $\hat{\beta}_T = -0.2240\%/y$, which is 3.5% more negative than that observed. Similarly, for individuals with ages in the interval [70, 95] years, accounting for mortality selection implies that the observed regression coefficient $\hat{\beta}_T = -0.2706\%/y$ (Table 2) should be ~4% more negative, that is, that the actual *BV* decrease rate $\hat{\beta}_T$ is about −0.281%/y.

Discussion

Although our CT segmentation approach (22) was tested, validated, and compared thoroughly to MRI, this study has limitations. The statistical comparison between Tsimane and the studies of European and U.S. samples relies on a comparison between CT-derived and MRI-derived volumes, respectively, rather than on random sampling and matching of participants scanned using the same neuroimaging modality. While different survival biases across Tsimane and reference samples are potential confounds, the small magnitude of the estimated mortality effect on the slope of *BV* as a function of age suggests that mortality selection alone is unlikely to account for the large differences in *BV* trajectory between Tsimane and reference samples. Nevertheless, because this study is cross-sectional, inferences on within-individual change in brain atrophy with age await longitudinal data. A total of 567 participants (76% of our sample) constituted 80% of the sample studied by Kaplan et al. (8), and 685 participants (92% of our sample) constituted 52% of the sample of Rowan et al. (32). Thus, although our sample is not identical to those of Kaplan et al. and Rowan et al., the biometric profiles of the 3 samples are likely similar insofar as inflammatory, cardiovascular, and metabolic parameters are concerned.

In conclusion, the Tsimane exhibit smaller age-related *BV* declines relative to industrialized populations, suggesting that their low CVD burden (8) outweighs their high, infection-driven inflammatory risk. If (a) the cross-sectional data (which we believe are population-representative of Tsimane adults aged 40 and older) represent well the average life course of individuals and if (b) the Tsimane are representative of the baseline case prior to urbanization, these results suggest a ~70% increase in the rates of age-dependent *BV* decrease accompanying industrialized lifestyles. Despite its limitations, this study suggests that brain atrophy may be slowed substantially by lifestyles associated with very low CVD risk, and that there is ample scope for interventions to improve brain health, even in the presence of chronically high systemic inflammation. Lastly, the slow rate of age-dependent *BV* decrease in the Tsimane raises new questions about dementia, given the role of both infections and vascular factors in dementia risk.

Funding

This work was supported by the National Institute on Aging at the National Institutes of Health (RF1 AG 054442 to H.K., C.E.F., and G.S.T.), as well as by the Institute for Advanced Study in Toulouse and the Agence Nationale

de la Recherche under the Investissements d'Avenir program (ANR-17-EURE-0010 to J.S.).

Conflict of Interest

None declared.

Author Contributions

Study design: A.I., M.G., J.S., B.C.T., M.D.G., G.S.T., C.E.F., and H.K. Subject recruitment: D.K.C., E.S., J.S., B.C.T., M.D.G., and H.K. Data collection: C.J.R., L.S.W., A.H.A., R.C.T., D.E.M., D.K.C., E.S., S.A., A.R.G., P.L.H., J.S., B.C.T., M.D.G., and H.K. Data curation: A.I., N.N.C., M.C., M.L.S., J.D.S., J.S., B.C.T., and H.K. Demographic data analysis: M.G., J.S., B.C.T., and M.D.G. Neuroimage analysis: A.I., N.N.C., D.J.R., K.A.R., A.S.M., N.F.C., M.C., V.N., E.M.L., H.C.C., M.L.S., and J.D.S. Statistical analysis: A.I., N.N.C., D.J.R., K.A.R., A.S.M., N.F.C., V.N., M.G., W.J.M., P.L.H., B.C.T., M.D.G., C.E.F., and H.K. Interpretation of the results: A.I., N.N.C., D.J.R., M.G., W.J.M., J.S., B.C.T., M.D.G., C.E.F., and H.K. Manuscript redaction: A.I., M.G., W.J.M., J.S., B.C.T., M.D.G., G.S.T., C.E.F., and H.K. All authors reviewed and approved the final version of the manuscript.

References

1. Manolio TA, Kronmal RA, Burke GL, et al. Magnetic resonance abnormalities and cardiovascular disease in older adults. The Cardiovascular Health Study. *Stroke*. 1994;25:318–327. doi:10.1161/01.str.25.2.318
2. Kim RE, Yun CH, Thomas RJ, et al. Lifestyle-dependent brain change: a longitudinal cohort MRI study. *Neurobiol Aging*. 2018;69:48–57. doi:10.1016/j.neurobiolaging.2018.04.017
3. Jefferson AL, Massaro JM, Wolf PA, et al. Inflammatory biomarkers are associated with total brain volume: the Framingham Heart Study. *Neurology*. 2007;68:1032–1038. doi:10.1212/01.wnl.0000257815.20548.df
4. Marsland AL, Gianaros PJ, Kuan DC, Sheu LK, Krajina K, Manuck SB. Brain morphology links systemic inflammation to cognitive function in midlife adults. *Brain Behav Immun*. 2015;48:195–204. doi:10.1016/j.bbi.2015.03.015
5. Sala-Llonch R, Idland AV, Borza T, et al. Inflammation, amyloid, and atrophy in the aging brain: relationships with longitudinal changes in cognition. *J Alzheimers Dis*. 2017;58:829–840. doi:10.3233/JAD-161146
6. Gu Y, Vorburger R, Scarmeas N, et al. Circulating inflammatory biomarkers in relation to brain structural measurements in a non-demented elderly population. *Brain Behav Immun*. 2017;65:150–160. doi:10.1016/j.bbi.2017.04.022
7. Hanning U, Roesler A, Peters A, Berger K, Baune BT. Structural brain changes and all-cause mortality in the elderly population—the mediating role of inflammation. *Age (Dordr)*. 2016;38:455–464. doi:10.1007/s11357-016-9951-9
8. Kaplan H, Thompson RC, Trumble BC, et al. Coronary atherosclerosis in indigenous South American Tsimane: a cross-sectional cohort study. *Lancet*. 2017;389:1730–1739. doi:10.1016/S0140-6736(17)30752-3
9. Blackwell AD, Trumble BC, Maldonado Suarez I, et al. Immune function in Amazonian horticulturalists. *Ann Hum Biol*. 2016;43:382–396. doi:10.1080/03014460.2016.1189963
10. Blackwell AD, Gurven MD, Sugiyama LS, et al. Evidence for a peak shift in a humoral response to helminths: age profiles of IgE in the Shuar of Ecuador, the Tsimane of Bolivia, and the U.S. NHANES. *PLoS Negl Trop Dis*. 2011;5:e1218. doi:10.1371/journal.pntd.0001218
11. Gurven M, Kaplan H, Crimmins E, Finch C, Winking J. Lifetime inflammation in two epidemiological worlds: the Tsimane of Bolivia and the United States. *J GerontolA Biol Sci Med Sci* . 2008;63A:196–199. doi:10.1093/gerona/63.2.196
12. Vasunilashorn S, Finch CE, Crimmins EM, et al. Inflammatory gene variants in the Tsimane, an indigenous Bolivian population with a high infectious load. *Biodemography Soc Biol*. 2011;57:33–52. doi:10.1080/19485565.2011.564475
13. Blackwell AD, Martin M, Kaplan H, Gurven M. Antagonism between two intestinal parasites in humans: the importance of co-infection for infection risk and recovery dynamics. *Proc Biol Sci*. 2013;280:20131671. doi:10.1098/rspb.2013.1671
14. Gurven M, Kaplan H, Supa AZ. Mortality experience of Tsimane Amerindians of Bolivia: regional variation and temporal trends. *Am J Hum Biol*. 2007;19:376–398. doi:10.1002/ajhb.20600
15. Gurven M, Blackwell A, Eid D, Stieglitz J, Kaplan H. Does blood pressure inevitably rise with age? Longitudinal evidence among forager-horticulturalists. *Hypertension*. 2012;60:25–33. doi:10.1161/HYPERTENSIONAHA.111.189100
16. Kaplan H, Thompson R, Trumble BC, et al. Indigenous South American Tsimane demonstrate the lowest levels of coronary atherosclerosis. *Lancet*. 2017;S0140:30752–30753. doi:10.1016/S0140-6736(17)30752–3
17. Vasunilashorn S, Crimmins EM, Kim J-K, et al. Blood lipids, infection, and inflammatory markers in the Tsimane of Bolivia. *J Hum Biol*. 2010;22:731–740. doi:10.1002/ajhb.21074
18. Gurven M, Jaeggi AV, Kaplan H, Cummings D. Physical activity and modernization among Bolivian Amerindians. *PLoS One*. 2013;8:e55679. doi:10.1371/journal.pone.0055679
19. Martin MA, Lassek WD, Gaulin SJ, et al. Fatty acid composition in the mature milk of Bolivian forager-horticulturalists: controlled comparisons with a US sample. *Matern Child Nutr*. 2012;8:404–418. doi:10.1111/j.1740-8709.2012.00412.x
20. Kraft TS, Stieglitz J, Trumble BC, Martin M, Kaplan H, Gurven M. Nutrition transition in 2 lowland Bolivian subsistence populations. *Am J Clin Nutr*. 2018;108:1183–1195. doi:10.1093/ajcn/nqy250
21. Stefanidis KB, Askew CD, Greaves K, Summers MJ. The effect of non-stroke cardiovascular disease states on risk for cognitive decline and dementia: a systematic and meta-analytic review. *Neuropsychol Rev*. 2018;28:1–15. doi:10.1007/s11065-017-9359-z
22. Irimia A, Maher AS, Rostowsky KA, Chowdhury NF, Hwang DH, Law EM. Brain segmentation from computed tomography of healthy aging and geriatric concussion at variable spatial resolutions. *Front Neuroinform*. 2019;13:9. doi:10.3389/fninf.2019.00009
23. Ashburner J, Friston KJ. Unified segmentation. *Neuroimage*. 2005;26:839–851. doi:10.1016/j.neuroimage.2005.02.018
24. Bishop CM. *Neural Networks for Pattern Recognition*. New York: Oxford University Press; 1995.
25. Collins DL, Holmes CJ, Peters TM, Evans AC. Automatic 3D segmentation of neuro-anatomical structures from MRI. *Hum Brain Map*. 1995;3:190–208. doi:10.1002/hbm.460030304
26. Evans AC, Kamber M, Collins DL, Macdonald D. An MRI-based probabilistic atlas of neuroanatomy. In: Shorvon SD, Fish DR, Andermann F, Bydder GM, Stefan H, eds. *Magnetic Resonance Scanning and Epilepsy*. Springer; 1994:263–274. doi:10.1007/978-1-4615-2546-2_48
27. Wedderburn RWM. Quasi-likelihood functions, generalized linear-models, and Gauss–Newton method. *Biometrika*. 1974;61:439–447. doi:10.1093/biomet/61.3.439
28. Schippling S, Ostwaldt AC, Suppa P, et al. Global and regional annual brain volume loss rates in physiological aging. *J Neurol*. 2017;264:520–528. doi:10.1007/s00415-016-8374-y
29. Vinke EJ, de Groot M, Venkatraghavan V, et al. Trajectories of imaging markers in brain aging: the Rotterdam Study. *Neurobiol Aging*. 2018;71:32–40. doi:10.1016/j.neurobiolaging.2018.07.001
30. Irimia A. Cross-sectional volumes and trajectories of the human brain, gray matter, white matter and cerebrospinal fluid in 9473 typically aging adults. *Neuroinformatics*. 2021;19:347–366. doi:10.1007/s12021-020-09480-w
31. Li X, Ploner A, Wang Y, et al. Longitudinal trajectories, correlations and mortality associations of nine biological ages across 20-years follow-up. *ELife*. 2020;9:1–20. doi:10.7554/eLife.51507
32. Rowan CJ, Eskander MA, Seabright E, et al. Very low prevalence and incidence of atrial fibrillation among Bolivian forager-farmers. *Ann Glob Health*. 2021;87:18. doi:10.5334/aogh.3252